Supporting Information

Redox-Active Phthalocyanine-Decorated Graphene Aerogels for High-Performance Supercapacitors Based on Ionic Liquid Electrolyte

Lifang Yang, Kelei Zhuo,* Xiaochao Xu, Zezhong Zhang, Quanzhou Du, Yujuan Chen, Dong Sun, and Jianji Wang* □

Henan Key Laboratory of Green Chemistry, Collaborative Innovation Center of Henan Province for Green Manufacturing of Fine Chemicals, Key Laboratory of Green Chemical Media and Reactions, Ministry of Education, School of Chemistry and Chemical Engineering, Henan Normal University, Xinxiang, Henan 453007, China.

Results and Discussion

1. H_3PO_4 role in the preparation

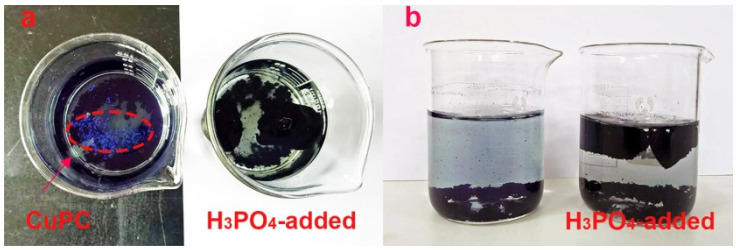

Figure S1. (a) Top view and (b) side view photos of the CuPC-rGA systems prepared with/without H_3PO_4 in the hydrothermal treatments.

As shown in Figure S1, CuPC was not fully reacted with rGA to form composites without the addition of H_3PO_4. This may be resulted from poor solubility of CuPC or PC in water. The introduction of H_3PO_4 would facilitate PC or CuPC more dissolvable at high temperature, and thus the CuPC or PC would be combined tightly with rGA via π-π interactions to form stable nanocomposites.

* Email: klzhuo@263.net, klzhuo@htu.cn, jwang@htu.cn

2. UV-vis absorption and FL spectroscopy

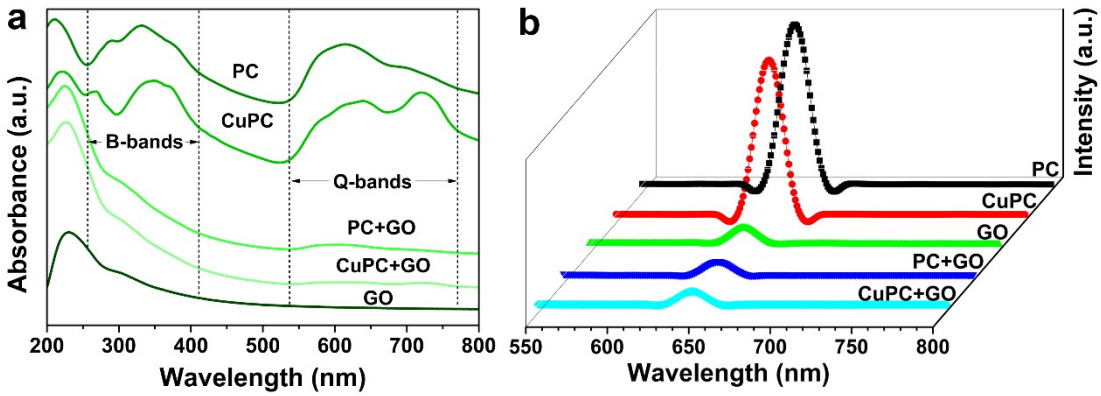

Figure S2. (a) UV-vis and (b) Fluorescence spectra of PC, CuPC, GO, PC+GO, and CuPC+GO in water.

To investigate the interaction between PC or CuPC molecules and GO sheets in advance, UV-vis absorption and fluorescence (FL) spectrometry were conducted (Figure S2). As illustrated in Figure S 2a, the GO dispersion displays a maximum absorption at 231nm resulting from the π-π* transition of aromatic C=C bonds and a shoulder peak around 300 nm arising from the n-π* transition of the sp^3 regions.[1] Both UV-vis absorption spectra of PC and CuPC in aqueous solution show two characteristic absorption bands (B-band at ca. 275 - 400 nm and Q-band at ca. 600 - 750 nm), which is ascribed to the π-π* transitions from HOMO and LUMO of PC and CuPC-ring.[2] After mixing with GO, the broadening and blue shift of B-band in the spectra of the PC + GO and CuPC+GO mixtures indicate the presence of non-covalent interaction between PC (or CuPC) and GO sheets.[3]

FL emission spectra of the samples at the same excitation wavelength (λ_{ex}= 320 nm) were recorded and are depicted in Figure S2b. PC, CuPC, GO, and PC+GO and CuPC+GO mixtures all show an emission peak around 643 nm. Owing to the electron transfer from PC (or CuPC) to GO, an obvious decrease in FL intensity is observed in the PC+GO and CuPC+GO mixtures when compared to PC and CuPC).[4] This phenomenon further confirms that PC and CuPC molecules can be grafted onto GO

surfaces by non-covalent π-π interactions between them, and thus provides a possibility of the successful preparation of PC-rGA and CuPC-rGA composites.[5]

3. Contact angle measurements

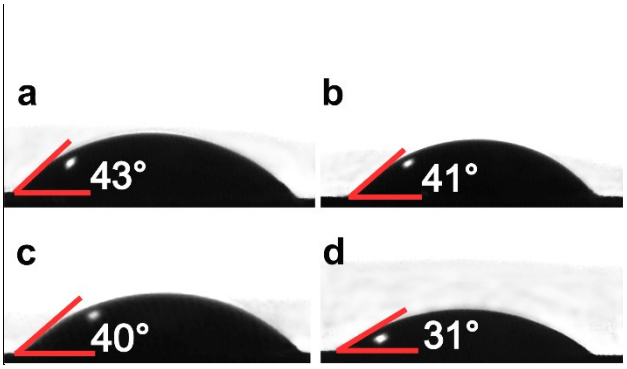

Figure S3. Contact angle measurements of $EmimBF_4$ toward HRGA (a) and $CuPC_x$-rGA (b-d). *x* refers to the concentration of CuPC added in the preparation process of the materials, *x* = 0.02 (b), 0.04 (c), and 0.06 mmol (d).

4. H_2SO_4 treated CuPC-rGA (S)

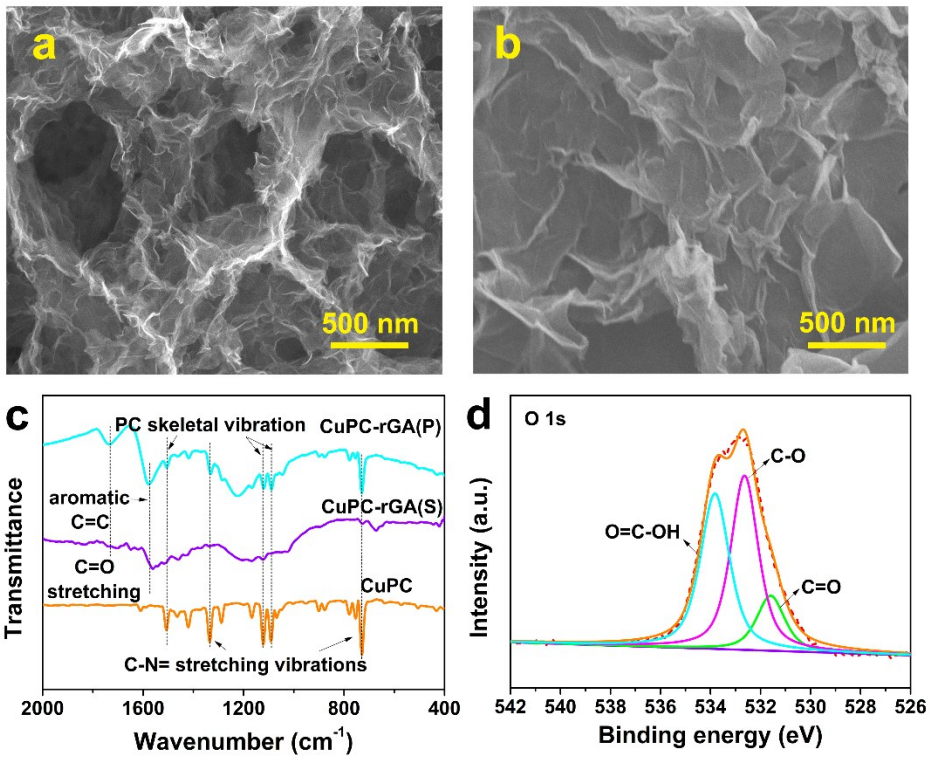

Figure S4. SEM images of CuPC-rGA and CuPC-rGA (S); (c) FTIR of CuPC, CuPC-rGA and CuPC-rGA (S); (d) O1s high-resolution of CuPC-rGA (S).

5. FT-IR spectroscopy

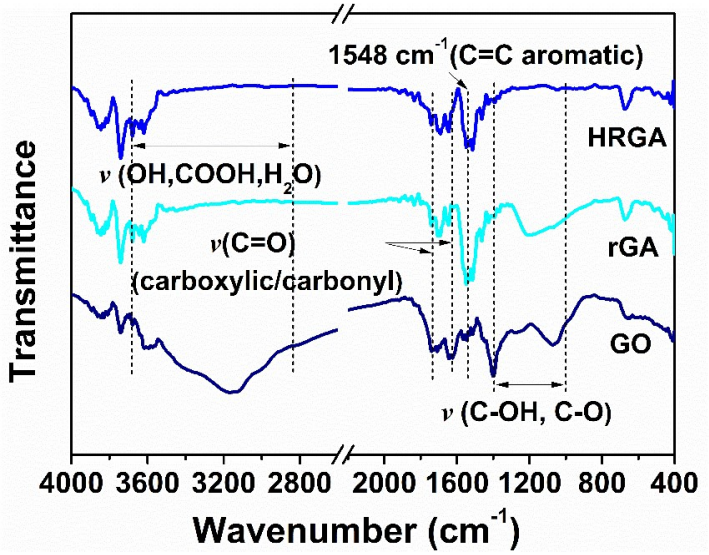

Figure S5. FT-IR spectra of blank GO, rGA, and HRGA

6. XPS analysis

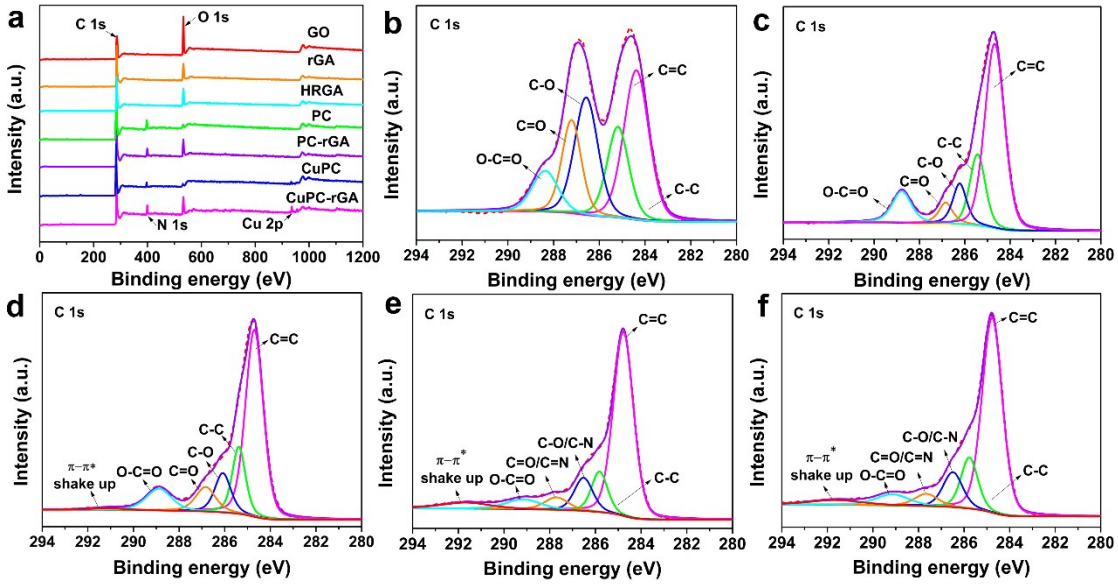

Figure S6. (a) XPS profiles of various samples; (b-f) Deconvoluted C 1s XPS spectra of GO, rGA, HRGA, PC-rGA, and CuPC-rGA.

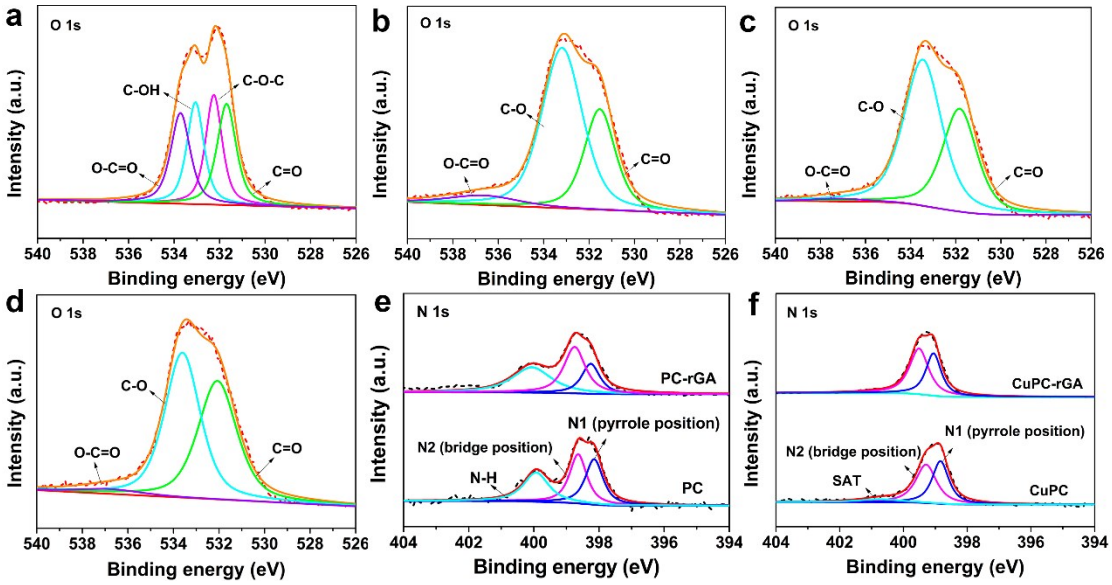

Figure S7. (a-d) O 1s high-resolution XPS spectra of rGA, HRGA, PC-rGA, and CuPC-rGA; (e-f) N1s high-resolution XPS spectra of PC, CuPC, PC-rGA, and CuPC-rGA.

Chemical compositions of the samples were provided by XPS measurements (Figure S6). As shown in Figure S 6b, the deconvoluted high-resolution C1s spectra of GO shows the featured bonding types: C=C (284.2 eV), C-C (284.9 eV), C-O (286.4 eV), C=O (287.2 eV), and O-C=O (288.4 eV).[6] Compared with GO, the peak intensities of aforementioned -CO- species show remarkable decreases in the core-fitted C 1s spectra of rGA and HRGA, as well as PC-rGA and CuPC-rGA composites. Moreover, the deconvoluted O 1s spectra consisting of four components are shown in Figure S 7a. Among the removed oxygen functionalities, the epoxy groups, failing to provide pseudocapacitance and hindering the electric conductivity, declined greatly in the rGA. And the H_3PO_4 addition accelerated the transformation of C-O-C into C-O, which would be favourable for enhancing the wettability of the materials as the electrode and also beneficial to the electrolyte transportation in the pores. In the nanocomposites, the new binding energy observed at 285.3 eV belongs to the C-N bond of PC or CuPC themselves (Figure S7e,f).[7] The aforementioned results indicate that no more fresh bonds are developed in the composites, further demonstrating the non-covalent decoration of graphene by PC or CuPC.

The percentages of the PC or CuPC components on the rGA surface were estimated on the elemental analysis from XPS experiments (Table S1). The elemental analysis shows that the content of N in both PC-rGA and CuPC-rGA was 7.44 wt% and 7.39 wt%, respectively. There are eight nitrogen atoms in the PC or CuPC macrocycle skeleton, and thus the content of PC or CuPC in the composites can be calculated to be (7.44÷14) ÷8*514.54=34.2% for PC-rGA or (7.39÷14) ÷8*576.07=38.0% for CuPC-rGA.

7. XRD analysis and Raman measurement

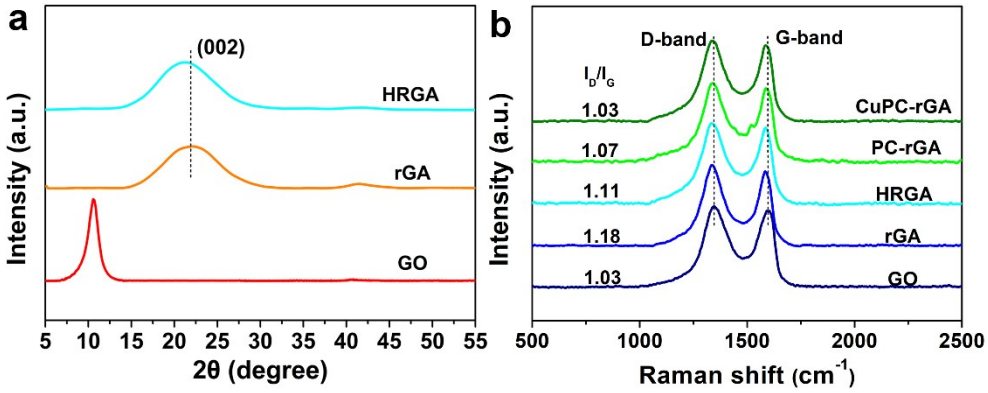

Figure S8. (a) XRD profiles of GO, rGA, and HRGA; (b) Raman spectra of various samples.

As seen from Figure S 8a, the GO sample displays the characteristic (001) reflection of carbonaceous at 2θ =10.6°, which is distinctly different from that of pristine graphite at 26.5°,[8] and the later entirely disappears after experiencing the hydrothermal process. Meanwhile, another broad diffraction peak at 22° is attributed to the (002) plane of graphene, the changes in diffraction patterns demonstrate a good conversion of graphite into GO and further reduction into rGA and HRGA through the partial elimination of oxygen-containing groups and restacking of few-layer graphene sheets. [9] It is worth noting that the diffraction peak (002) of HRGA shifts to a lower angle, indicating a larger interspace by Bragg's Law ($2d\sin\theta = n\lambda$). This observation may be explained by

the enhanced quinone-type oxygen on rGA surfaces owing to the addition of H_3PO_4. [10]

Two characteristic Raman signals, D band centred at 1349 cm^{-1} and G band at 1580 cm^{-1}, are ascribed to the defects and disorder in the graphitic structure, and the E_{2g} in-plane vibration of sp^2 carbon atoms. [10] The value of I_D/I_G, which can be used to assess the graphitization degree of the carbon materials, increases from GO to PC-rGA, as indicated in Figure S 8b. The slightly reduced ratio in CuPC-rGA can be attributed to the improved graphitic domains or the overlap of HRGA with the C=C vibration of CuPC macro-ring. Moreover, the similar peak positions suggest that the conjugated network of graphene sheets is slightly disrupted by the introduced PC or CuPC. [11]

8. Brunauer-Emmett-Teller (BET)

Table S1. Specific surface areas (S_{BET}) and elemental compositions of rGA, HRGA, PC-rGA, and CuPC-rGA.

Sample	S_{BET}[a]	$S_{t\text{-}plot}$[b]	A[c]	V_{BJH}[d]	Pore width	Elemental content (%)			
	($m^2\ g^{-1}$)	($m^2\ g^{-1}$)	(%)	($m^3\ g^{-1}$)	(nm)	C	N	O	Cu
rGA	277.0	84.4	30.4	0.42	6.25	85.6		14.4	
HRGA	338.9	93.8	27.6	0.44	7.09	83.8		16.2	
PC-rGA	207.1	69.3	33.5	0.45	14.42	82.1	7.44	10.5	
CuPC-rGA	192.9	44.6	23.2	0.51	18.36	80.9	7.39	10.7	0.99

[a] Specific surface area determined by BET method. [b] Microporous surface area by t-plot method. [c] Percent of microporous surface area. [d] BJH adsorption pore volume.

Table S2. Comparison of the electrochemical performance of PC –rGA and CuPC-rGA based SCs with other functionalized graphene-based devices.

Devices	Electrolyte	*ΔV/V*	Energy density (W h kg^{-1})	Power density (W kg^{-1})	Cycles	Retention	Ref
G-FePC// G-FePC	Na_2SO_4	0.7	59	315	2000	100% at 5 A g^{-1}	[30]
AQS-rGA//RuO_2-rGA	H_2SO_4	0.6	31.9	1671.7	5000	76% at 5 A g^{-1}	[48]
SWNT/MnO_2//SWNT/MnO_2	$TEABF_4$/PC	3	70	77.3	1000	98.5% at 2 A g^{-1}	[49]
AC// MnO_X-rGO	$EmimBF_4$	2.7	47.9	270	8000	96% at 5 A g^{-1}	[51]
STC//STC	$EmimBF_4$	3.5	76	200	10000	90% at 10 A g^{-1}	[50]
FeOOH//APDC f-SSC	$EmimNTF_2$	2.5	17.9	1500	2000	80.5% at 1 A g^{-1}	[52]
Fe_2O_3-GNS//APDC	$EmimBF_4$	4	177	200	2000	81.5% at 1 A g^{-1}	[26]
AC//AC	$EmimBF_4$	4	92	1000	10000	92.2% at 5 A g^{-1}	[47]
NS-GA//NS-GA	$EmimBF_4$	3.8	100.7	940	3000	90% at 2 A g^{-1}	[53]
PC-rGA//PC-rGA	$EmimBF_4$	4	107	1000	8000	82.1% at 1 A g^{-1}	This work
CuPC-rGA//CuPC-rGA	$EmimBF_4$	4	111	1009	8000	83.6% at 1 A g^{-1}	This work

9. CVs and GCD profiles

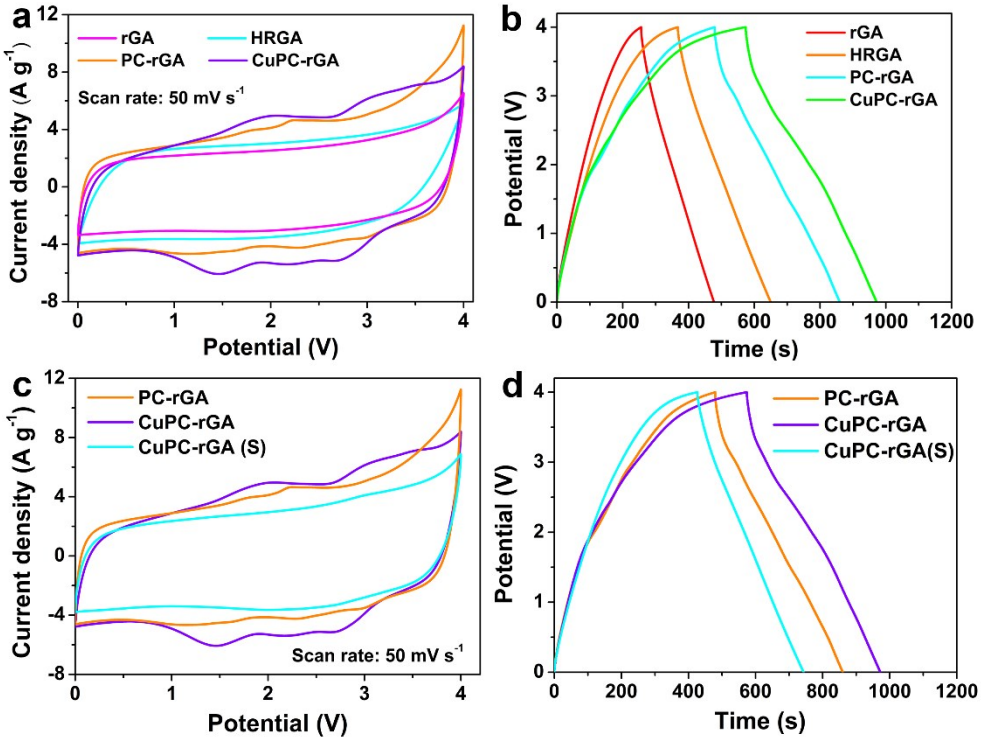

Figure S9. (a) CV and (b) GCD curves of rGA, HRGA, PC-rGA, and CuPC-rGA; (c) CV and (d) GCD comparison of different of different acid treated CuPC-rGA.

10. Bode plots

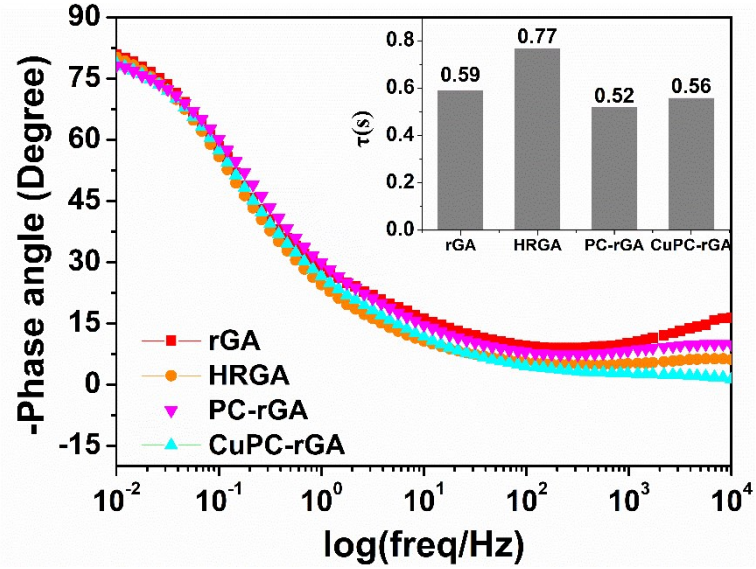

Figure S10. Bode plot of rGA, HRGA, PC-rGA and CuPC-rGA.

11.Energy effecience

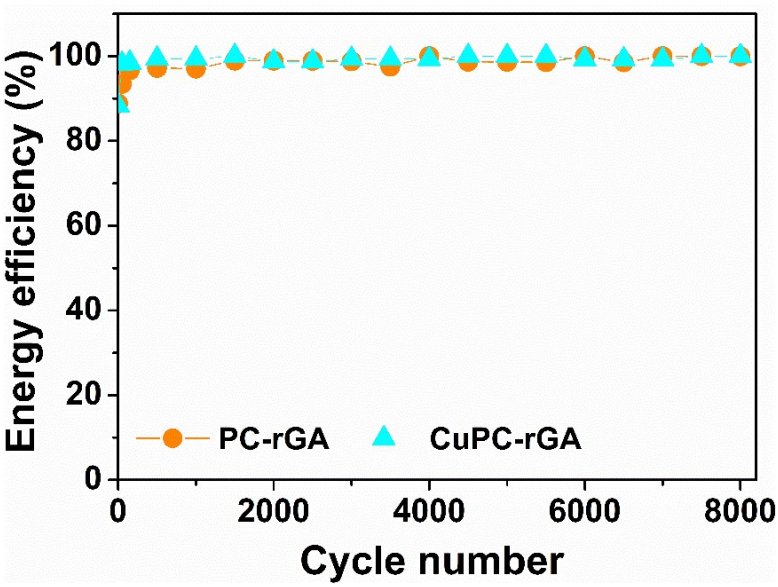

Figure S11. Energy efficiency of PC-rGA and CuPC-rGA at 1 A g^{-1}.

12. Charging-discharging mechanism

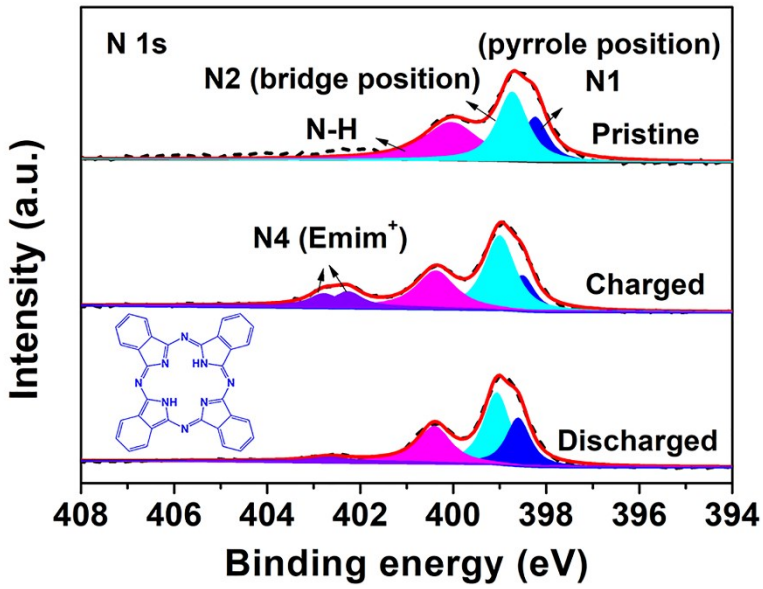

Figure S12. N 1s high-resolution XPS spectra of PC-rGA as the electrode material for supercapacitors in $EmimBF_4$ as the electrolyte before/after charging/discharging.

References

1. Z. Sun, H. Fu, L. Deng and J. Wang, *Anal Chim Acta*, 2013, **761**, 84-91.
2. K. P. Madhuri and N. S. John, *Applied Surface Science*, 2018, **449**, 528-536.
3. Y. Shabangoli, M. S. Rahmanifar, M. F. El-Kady, A. Noori, M. F. Mousavi and R. B. Kaner, *Advanced Energy Materials*, 2018, **8**, 1802869-1802880.
4. G. B. Markad, N. Padma, R. Chadha, K. C. Gupta, A. K. Rajarajan, P. Deb and S. Kapoor, *Applied Surface Science*, 2020, **505**, 144624-144633.
5. G. Chen, H. Shi, F. Ban, Y. Zhang and L. Sun, *Microchimica Acta*, 2015, **182**, 2469-2476.
6. H. Li, Y. Zhao, S. Liu, P. Li, D. Yuan and C. He, *Microporous and Mesoporous Materials*, 2020, **297**, 109960-109968.
7. Y. Han, T. Wang, T. Li, X. Gao, W. Li, Z. Zhang, Y. Wang and X. Zhang, *Carbon*, 2017, **119**, 111-118.
8. S. Yang, K. Zhuo, D. Sun, X. Wang and J. Wang, *J Colloid Interface Sci*, 2019, **543**, 263-272.
9. M. S. Lee, D. R. Whang, Y. H. Song, J. T. Kim, M. H. Yang, U. H. Choi and D. W. Chang, *Carbon*, 2019, **152**, 915-923.
13. H. Ma, Q. Zhou, M. Wu, M. Zhang, B. Yao, T. Gao, H. Wang, C. Li, D. Sui, Y. Chen and G. Shi, *Journal of Materials Chemistry A*, 2018, **6**, 6587-6594.
14. R. Shi, C. Han, H. Duan, L. Xu, D. Zhou, H. Li, J. Li, F. Kang, B. Li and G. Wang, *Advanced Energy Materials*, 2018, **8**, 1802088-1802096.